Available online at www.sciencedirect.com
ScienceDirect
Tectonophysics 427 (2006) 73–93
TECTONOPHYSICS
www.elsevier.com/locate/tecto

On the role of grain topology in dynamic grain growth — 2D microstructural modeling

A. Kellermann Slotemaker *, J.H.P. de Bresser

HPT Laboratory, Department of Earth Sciences, Faculty of Geosciences, Utrecht University, P.O. Box 80.021, 3508 TA Utrecht, The Netherlands

Received 1 July 2005; received in revised form 8 February 2006; accepted 18 May 2006
Available online 7 September 2006

Abstract

Microstructural modification processes like dynamic recrystallization and grain growth can have a major effect on the transient and (semi-)steady state flow behaviour of deforming materials. Work on metals and ceramics suggests that deformation-enhanced changes in grain topology and the corresponding increase in fraction of non-hexagonal grains, called cellular defect fraction, can promote grain growth during deformation. The present study tests this hypothesis, by investigating the evolution of the cellular defect fraction during deformation, accompanied by grain growth, of aggregates with distributed grain sizes. For this purpose, we made use of the ELLE 2D microstructural modeling package. We simulated and quantified microstructural evolution under conditions where both surface energy driven grain boundary migration (GBM) and homogeneous deformation or grain size sensitive (GSS) straining were allowed to occur. The simulations show that contemporaneous GBM and simple geometrical straining of grain aggregates with distributed grain size and coordination number lead to extra grain neighbor switching, an increase in defect fraction, and enhanced grain growth. An increase in defect fraction was also found in a selected set of natural calcite mylonites that, with increasing temperature, show an increase in grain size and contribution of GSS creep. Analysis of defect fraction thus appears to be a good microstructural tool to establish whether or not a material has experienced normal static (defect fraction ~0.7) or dynamic grain growth (defect fraction ~0.8).

Keywords: Grain growth; Deformation; Topology; Aspect ratio

1. Introduction

1.1. Background and general problem statement

Microstructural modification processes like dynamic recrystallization and grain growth can have a major effect on the transient and (semi-)steady state flow behaviour of deforming materials. For example, high strain (torsion) experiments on coarse-grained olivine (Bystricky et al., 2000) and calcite materials (Schmid et al., 1987; Rutter, 1995, 1998; Pieri et al., 2001; Barnhoorn et al., 2004) have demonstrated transient strain weakening related to grain refinement by dynamic recrystallization. Relatively high shear strains were needed to approach steady state flow. Materials with relatively small starting grain sizes may, on the other hand, show strain hardening related to ongoing grain coarsening (e.g., olivine materials: Karato et al., 1986; Hirth and Kohlstedt, 1995). Evidently, meaningful modeling of large strain flow in the Earth must take into account microstructural evolution effects

* Corresponding author. Tel.: +31 30 2534976 (Office); fax: +31 30 2537725.
E-mail address: arthur@geo.uu.nl (A. Kellermann Slotemaker).

0040-1951/$ - see front matter © 2006 Elsevier B.V. All rights reserved.
doi:10.1016/j.tecto.2006.05.017

that cause rheological changes (e.g., Braun et al., 1999; Urai and Jessell, 2001; Montesi and Hirth, 2003; Yamasaki, 2004). This requires a mechanism-based understanding of microstructure modification processes.

In a recent experimental study (Kellermann Slotemaker et al., 2004), we deformed fine-grained synthetic forsterite aggregates at a strain rate of 5×10^{-6} s^{-1}, 600 MPa confining pressure and a temperature of 950 °C. Under these conditions, the forsterite material deforms by a grain size sensitive (GSS) creep mechanism involving grain boundary sliding (GBS), after McDonnell et al. (1999). We observed strain hardening in the stress–strain curves as well as an increase in grain size during the experiments. More importantly, comparison of the results of the deformation tests with heat treatment (static) tests showed that grain growth was strain-dependent (i.e. dynamic) rather than time-dependent (cf. static grain growth). No lattice preferred orientation developed in the samples (Kellermann Slotemaker et al., 2004) and only little evidence was found for dislocation activity on TEM scale (McDonnell et al., 1999). We thus concluded that grain boundary migration (GBM) in the material, resulting in dynamic grain growth (DGG), was dominantly surface energy driven. It is known from metals and ceramics that DGG and GSS creep, with a strong GBS signature, are intimately related processes (Seidensticker and Mayo, 1998a). Models by Sato et al. (1990) and Sherwood and Hamilton (1992, 1994) propose that grain (neighbor) switching during GBS (after Ashby and Verrall, 1973) may increase the probability of high-sided grains coming in contact with low-sided grains, in turn stimulating grain growth. Sherwood and Hamilton (1992, 1994) hypothesized that deformation-induced grain neighbor switching results in changes in grain topology, i.e. an increase in the fraction of non-hexagonal grains (in 2D), called the cellular defect fraction (originally defined by Hillert, 1965). Indeed, measurements of grain topology in the forsterite samples showed an increase of the cellular defect fraction with increasing strain, consistent with the increase in grain size and related strain hardening.

The results of the experimental study on synthetic forsterite (Kellermann Slotemaker et al., 2004) corroborate the importance of understanding microstructure modification during flow of Earth materials. However, it is as yet not clear if analysis of the cellular defect fraction is a useful and generally applicable tool to identify DGG in relation to grain neighbor switching and deformation. It is the broad objective of the present paper to shed light on this. We used the 2D numerical modeling package ELLE (Jessell et al., 2001) to simulate combined deformation and surface energy driven GBM, specifically aiming (a) to investigate the evolution of cellular defect fraction with strain and time in relation to grain growth with or without contemporaneous deformation, and (b) to test the hypothesis that extra neighbor switching induced by deformation causes an increase in cellular defect fraction, which in turn leads to enhanced grain growth. In our approach, we tested homogeneous 'geometrical' deformation as well as simulated inhomogeneous GSS creep. By 'geometrical' deformation we simply mean bulk homogeneous straining of the complete aggregate, i.e. as if the grain boundaries are completely passive elements in the aggregate. This deformation type is useful since it allows a straightforward approach to investigate the effect of changes in grain boundary geometry on grain growth. The effects of inhomogeneous GSS creep are less straightforward to interpret but are more applicable to the results of the forsterite work and other experimental studies on real materials.

Limited previous modeling work has been performed on combined homogeneous or inhomogeneous deformation and GBM. Bons and Urai (1992) studied simultaneous operation of surface energy driven GBM and homogeneous area-conservative deformation using a simple 2D network model. They demonstrated that syn-deformational grain growth slows down the progressive increase in aspect ratio normally associated with development of a shape-preferred orientation during homogeneous straining. However, they also found that if a grain shape preferred orientation is present, it slows down grain growth. Using a similar type of 2D modeling, Bate (2001) focused on the effect of deformation on GBM in nominally Zener-pinned microstructures and observed DGG, which he ascribes to deformation induced perturbations of the grain boundary geometry. The present study forms the next step forward by applying a modeling approach similar to Bons and Urai (1992) and Bate (2001), but looking in detail at (and quantifying) geometrical changes in grain topology, in particular defect fraction, which in turn link up with analytical neighbor switching models of Sherwood and Hamilton (1992, 1994) and Sato et al. (1990).

In this study, we explicitly excluded any grain size reduction mechanism contributing to grain size evolution. As such, the results are not directly applicable to (high) strain zones where dynamic recrystallized grains resulted from competition between grain size reduction and grain growth. The results could, however, apply to shear zones which experienced significant grain size reduction, causing rocks to switch in deformation mechanism to dominant GSS creep. Rather than ongoing grain size reduction, the continued microstructural evolution in such a shear zone would dominantly involve normal (or dynamic) grain growth (e.g. Herwegh et al., 2005).

The paper starts with a brief overview of dynamic grain growth theories presented in the literature, followed by an outline of our modeling approach. We then present the results of the modeling runs and assess how the present and previous modeling studies relate to the analytical approaches of grain neighbor switching. Finally, we discuss what factors need to be considered in future studies of DGG and make a comparison with natural rocks through defect fraction analysis on microstructures of selected carbonate mylonite samples, which were already extensively studied by Herwegh et al. (2005).

1.2. Dynamic grain growth models

Various experimental and modeling studies on grain growth behaviour during deformation have been performed (e.g. geological materials: Schmid et al., 1977; Karato et al., 1986; Walker et al., 1990; metals and ceramics: Holm et al., 1977; Holm et al., 1993; Sherwood and Hamilton, 1994; Seidensticker and Mayo, 1998a; modeling studies: Wilkinson and Caceres, 1984; Sato et al., 1990; Sherwood and Hamilton, 1992, 1994; Rabinovich and Trifonov, 1996; Seidensticker and Mayo, 1998b; Kim et al., 1999; Kim and Hiraga, 2000; Bate, 2001; Haslam et al., 2003). The following points emerged as being important in explaining DGG: (a) GBM kinematics, (b) deformation mechanisms, (c) deformation 'mode', i.e. homogeneous vs. inhomogeneous, and aspect ratio formation, and (d) topological changes. These points will be discussed in more detail below, with particular emphasis on the last aspect, in line with the aims of our study.

1.2.1. GBM kinematics

In materials that show fast grain boundary migration under static conditions, a dynamic component induced by deformation may contribute little to the overall grain growth and, hence, will be hard to recognize. Consequently, DGG is usually recognized in materials in which static grain growth is very slow or pinned due to the presence of one or more pinning phases (Seidensticker and Mayo, 1998a; Bate, 2001). Zener pinning can be established by the presence of relatively small-scale solutes and impurities at the grain boundary or by larger scale discrete particles or pores included within the grain matrix (Evans et al., 2001). Depending on the size of a pinning phase relative to the average matrix grain size, an average uniform (small sized pinning phase) or varying non-uniform (large sized pinning phase) Zener drag must be accounted for. In turn, this variation in pinning geometry may have a large effect on the net result of combined deformation and GBM (Bate, 2001). In materials with fast static grain growth, a dynamic component might well be present, but may contribute little to the overall grain growth. In natural rocks, Zener pinning is a common feature (Olgaard, 1990; Mas and Crowley, 1996; Krabbendam et al., 2003; Herwegh and Berger, 2004). In such rocks, dynamic grain growth may provide a significant contribution to the total grain growth.

1.2.2. Deformation mechanisms

Some DGG models specifically focus on how physical properties of GSS (diffusion) creep, whether or not combined with GBS, can result in enhanced migration of grain boundaries on the grain scale (Kim et al., 1999; Kim and Hiraga, 2000) and down to the atomistic scale (Haslam et al., 2003, 2004). Other models focus on the effects of accommodation by GBS. This mechanism may induce excess vacancies or dislocations in the grain boundary region, which can increase grain boundary mobility (Clark and Alden, 1973; Rabinovich and Trifonov, 1996) or the driving force for GBM (Wilkinson and Caceres, 1984). Since our motivation for doing the current study came from the results on forsterite, which did not show evidence that production of dislocations or excess vacancies in the grain boundary region played a role, it will not be considered further in this paper.

1.2.3. Deformation 'mode' and aspect ratio formation

Homogeneous 'geometrical' deformation is a simplified way of strain accumulation and is not related to a deformation mechanism with a specific microphysical basis. Nevertheless, this type of deformation allows straightforward straining of grain aggregates resulting in an increasing aspect ratio and associated development of a grain shape preferred orientation. In combination with GBM, homogeneous deformation has been shown to cause accelerating (Bate, 2001) as well as decelerating effects (Bons and Urai, 1992) on grain growth. More realistic modeling of deformation necessarily needs to take into account inhomogeneous straining to some extent, assuming a distributed grain size and a specific GSS (diffusion with or without GBS) or GSI (dislocation) creep mechanism. This will introduce a variable level of heterogeneity in the accommodation of strain between and/or within grains, which also may influence aspect ratio formation (Bate, 2001).

1.2.4. Topological changes

Related to this are the various forms of grain neighbor switching 'events' and changes in distribution of grain coordination number and cellular defect fraction (Sato et al., 1990; Sherwood and Hamilton, 1992). Grain neighbor switching related models on static and dynamic grain growth specifically base their grain growth (rate)

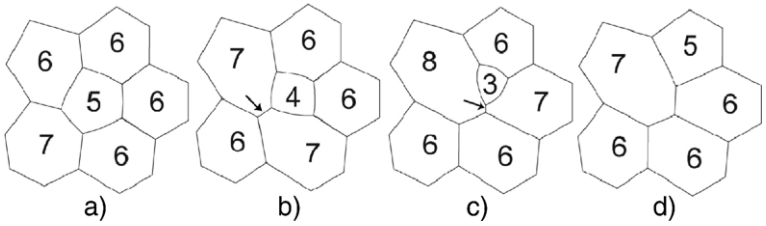

Fig. 1. Schematic drawing showing the evolution of a group of six grains undergoing surface energy driven GBM and neighbor switching, resulting in normal grain growth (after Fig. 4 of Hillert, 1965); coordination number is shown within each grain. Average coordination number remains 6 at all shown stages. Defect fraction is shown at each stage. (a) The initial state with two defects, i.e. one 5- and one 7-sided grain, $X_d = 2/6 = 0.33$. (b) The 5-sided grain has become 4-sided due to a neighbor switch (arrow), $X_d = 3/6 = 0.50$. (c) The 4-sided grain has become 3-sided due to another switch (arrow), $X_d = 3/6 = 0.50$. (d) Finally the 3-sided grain has disappeared and thus net grain growth has taken place $X_d = 2/5 = 0.40$. Note a 5- and a 7-sided grain are still present in the final state.

relations as a function of time (Hillert, 1965), strain (Sato et al., 1990) and strain rate (Sherwood and Hamilton, 1992, 1994; Seidensticker and Mayo, 1998b) on the various ways of grain neighbor switching. Such switching events can be considered as variants of defect 'climb' and 'glide' in analogy to the atomistic dislocation theory. Measures to describe grain topology are the arithmetic mean and second moment, i.e. the standard deviation, of the coordination number distribution (e.g. Weaire and Kermode, 1983; Anderson, 1988; Bons, 1993). Defect fraction is an additional way to describe the state of the coordination number distribution with a single value. Recalling Von Neumann's rule (1952), in two dimensions a 5-sided or lower coordinated grain will tend to shrink while a 7 or higher sided grain will tend to grow (Fig. 1). After a neighbor-switching event, there is a chance that grains changed their coordination number, resulting in a higher or lower defect fraction. According to Hillert (1965), neighbor switching during normal grain growth (Fig. 1), i.e. surface energy driven GBM without any deformation, occurs at a characteristic constant defect fraction of 0.75. Note that, although the defect fraction is constant, the absolute number of defects must decrease, given that the total number of all grains in the system decreases with net grain growth. Individual grains may switch back and forth from defect (non-hexagonal) to hexagonal coordination, depending on the evolution of migrating boundaries of neighboring grains. When deformation, e.g. by some combination of GBS and diffusion creep, occurs alongside normal grain growth, this can introduce extra neighbor switching events (Fig. 2), resulting in a change in defect fraction away from the steady state value of 0.75 for normal grain growth. If a higher fraction is produced, enhanced grain growth is expected. The latter forms the rationale for an analytically derived relation between strain rate and DGG rate presented by Sherwood and Hamilton (1992, 1994), expressed as:

$$\dot{d}_{\mathrm{dyn}} = \lambda \cdot d \cdot \dot{\varepsilon} \tag{1}$$

where $\dot{d}_{\mathrm{dyn}}$ is the DGG-rate, λ is a rate-parameter, d is the instantaneous average grain size and $\dot{\varepsilon}$ is the strain rate. Note that d can vary between different grain growth experiments as well as within a single experiment. Thus, in practice, data are best compared by normalizing (1) by the instantaneous average grain size (Seidensticker and Mayo, 1998a):

$$\frac{\dot{d}_{\mathrm{dyn}}}{d} = \lambda \cdot \dot{\varepsilon} \tag{2}$$

According to the model of Sherwood and Hamilton (1992), the value of the rate-parameter λ largely depends on the defect fraction, X_d, as they show that:

$$\lambda = k' \cdot X_d \tag{3}$$

where k' is a scaling constant.

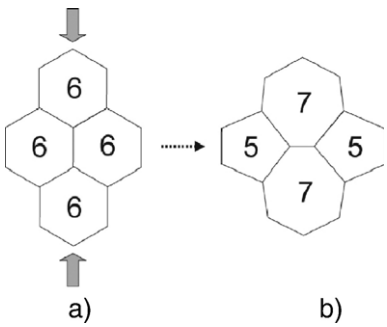

Fig. 2. Schematic illustration of deformation (GBS + diffusion) induced neighbor switching; coordination number is shown within each grain. (a) Initial state with four 6-sided grains being subjected to vertical compression, $X_d = 0/4 = 0.0$. (b) Final state after deformation and neighbor switching as top and bottom grains have become direct neighbors and both gained an extra side, while the two middle grains have been separated and both lost a side, $X_d = 4/4 = 1.0$ (after Sherwood and Hamilton, 1994, their Fig. 6).

From the above list of parameters that are of importance in DGG, we concentrate on changes in topology and, to a lesser extent, on changes in aspect ratio (and related deformation 'mode'), since these are potentially useful as measurable microstructural parameters. In the approach of Sherwood and Hamilton (1992), DGG is simply a response to extra neighbor switching and increasing defect fraction induced by some deformation event, irrespective of which physical processes are actually involved in the neighbor switching. Therefore, as a first order approach, it appears reasonable to model GBM in combination with simple homogeneous deformation, which allows an unambiguous investigation of geometric effects of deformation on defect fraction evolution and grain growth. Moreover, results are directly comparable to studies by Bons and Urai (1992) and Bate (2001), which have already proven this to be a successful way to simulate static grain growth and DGG. However, these investigations did not include quantitative analysis of topological changes during their simulations. A logical next step would be to perform GBM combined with inhomogeneous GSS creep simulations, which potentially predict more realistic topological changes. The theory of Sherwood and Hamilton (1992, 1994) on DGG predicts extra neighbor switching by GBS and possible related changes in coordination number distribution and defect fraction for dynamically grown material. However, to our knowledge, not many constraints are yet established on the dependence of defect fraction on deformation, leaving the value of λ in (1)–(3) with a large uncertainty. Our approach will supply a first order calibration of such variation in defect fraction, X_d (3).

2. Method

2.1. General approach

Grain microstructures of heat-treated and deformed material can be analyzed to quantify defect fraction using conventional image analysis techniques. Similarly, 2D simulations allow quantification and systematic investigation of various microstructural parameters, like defect fraction, and their evolution. Such microstructural analysis forms a powerful tool to test neighbor switching based DGG theories and verify/calibrate the variation in defect fraction under conditions of combined GBM and deformation. We concentrated on single-phase material.

We used the 2D microstructural modeling package ELLE to perform the simulations. This package provides a variety of routines to simulate individual microprocesses. In principle, ELLE is based upon a two-dimensional network structure in which grains are represented by polygons, and polygons are in turn defined by a closed set of connected nodes (see Fig. 3, modified after Piazolo, 2001). Straight boundary segments connect the nodes, of which there are two types, i.e. double nodes, connected to two neighboring nodes and triple nodes, connected to three neighboring nodes (Fig. 3). The latter reside at a triple point, where boundaries between three neighboring grains merge into one point. Average distance between nodes is controlled by user-defined parameters. The minimum allowed distance between two nodes, referred to as 'switchdistance', is set to a fixed value in all tests and maximum node separation is defined as 2.2 × switchdistance. In the general case where separation is lower or higher than this range, nodes are removed or added, respectively. If separation between two triple nodes is below the minimum they will switch neighbors rather than remove one of the triple nodes. The modeled area is a square finite element map (area set to 1000) with periodic boundaries, i.e. it is continuous on opposite sides of the frame. In this way, boundary effects are avoided as long as the modeled

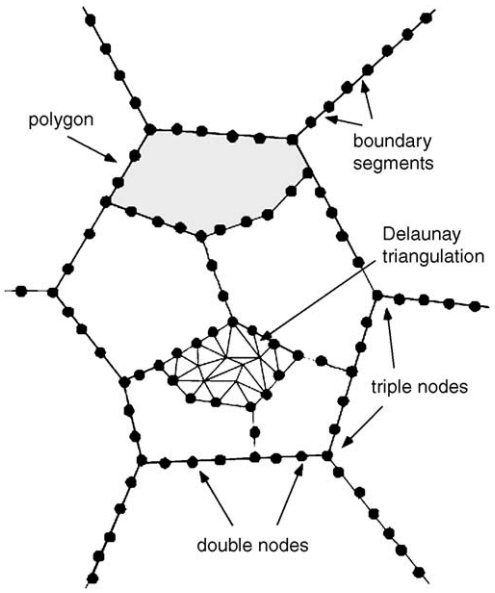

Fig. 3. Representation of the 2D finite element map of a grain aggregate (modified after Piazolo, 2001, see her Fig. 3.2). Each polygon domain (e.g. the light-gray area) forms a grain, which can be assigned a number of properties, such as viscosity. All polygons can, if desired, be triangulated to smaller elements using a Delaunay triangulation routine. This triangulation is, in contrast to the polygons, nodes and boundary segments, not permanent and can be used temporarily e.g. for the *basil* deformation routine. Triangulation elements may also have individual properties, including the stress and strain state during deformation.

polygonal network is sufficiently fine-grained. For more detailed information on the ELLE system, the reader is referred to Jessell et al. (2001) and the ELLE website (http://www.microstructure.info).

We effectively simulated contemporaneous activity of deformation and GBM by iteratively combining small strain and time steps of each separate process. To perform small steps of homogeneous deformation we used an ELLE routine named *elle_manuel*. This routine simulates homogeneous simple shear deformation. Shear strain step size is set as a displacement-value in the x-direction of the finite element map. The ELLE routine *elle_gg* is used to simulate surface energy driven GBM. *elle_gg* allows a quick (short computation times) evaluation of surface energy driven GBM, without the need to specify values for time, temperature and pressure, or material parameters like grain boundary mobility and activation energy for GBM. For a single boundary node, local boundary curvature, w, is defined as $1/R$, where R is the radius of an imaginary circle fitted through the specific node and its 2 neighboring boundary nodes. This curvature, w, forms the local driving force for GBM and is used to calculate the node-displacement, movdist, per stage (i.e. the time-unit) according to the following relation:

$$\text{movdist} = w \cdot M \tag{4}$$

where M is a rate-constant comparable to GBM mobility, defined as:

$$M = \text{speed\_up} \cdot \text{switchdistance}^2 \cdot 0.02 \tag{5}$$

In (5) speed_up limits the distance a node may move in any one *stage* and 0.02 is a fixed constant allowing the value for speed_up to vary within the range 0.3–1. As switchdistance is kept constant in all simulations, the value of M can only be varied by artificially changing the speed_up-value. In (4) a maximum value for movdist is set at 0.2 × switchdistance to prevent large node movements, in case of strong acute angles between nodes, which could destabilize the network. The movement calculation is done for each boundary node within each *stage*, where a 'GBM time step' consists of a specified number of *stages*. The program outputs mean statistics on grain size, grain shape and other parameters at a preset interval of stages.

We used *basil*, which is a finite element code for calculating viscous deformation developed separately from the Elle code (Barr and Houseman, 1992, 1996), to simulate inhomogeneous GSS deformation. During a *basil* deformation step, the polygonal network temporarily requires Delaunay triangulation (see Fig. 3). *basil* simulates simple shear deformation like *elle_manuel*, but rather than homogeneously deforming the microstructure (i.e. applying uniform viscosity), the program permits a spatially variable Newtonian (or non-Newtonian) viscosity. This way *basil* can model deformation of an aggregate with variable internal viscosity as also done by previous workers (Bons et al., 1997; Piazolo et al., 2002; Jessell et al., 2004, 2005). Each grain in a (starting) microstructure can be assigned a specific viscosity-value depending on user-defined parameters. Using this approach Piazolo (2001) and Piazolo et al. (2002) calculated a dislocation density dependent viscosity for each grain as:

$$\eta = \eta_{\text{base}} + \rho^{1/2} \tag{6}$$

where ρ is the dislocation density and η_{base} is a base viscosity specific to temperature, pressure conditions, and mineral species. In the present study, it was not our intention to model real values for viscosity corresponding to a specific material and natural conditions. Rather, our goal was to get a crude impression of the effect of spatially variable viscosity in comparison to simple homogeneous deformation. We applied the same approach as in (6) (by Piazolo et al., 2002), and calculated a grain size dependent viscosity, according to the following relation:

$$\eta = c \cdot d^3 \tag{7}$$

where d is the grain size, calculated as the equivalent circular diameter of the grain area, and c is a scaling-factor (arbitrarily set to 10^4). The grain size exponent is chosen to be 3, a typical value for grain boundary diffusion controlled creep. In practice, the approach in relation (7) allowed us to model deformation with relative viscosity differences between larger and smaller grains up to four orders of magnitude (for the fine-grained starting microstructure), similar to grain size dependent Newtonian creep. It is emphasized that this sort of modeling of GSS deformation is not based on any specific physical process; we simply imply grain size dependence through an intrinsic variable viscosity definition. After each GBM step, and before the following *basil* deformation step, we recalculated the viscosity value for each grain, as some grains may have grown, while others may have shrunk. *basil* requires input of boundary conditions on traction (stress) and/or velocity. Maximum strains of the order of 100% are possible.

During every simulation, intermediate output files were saved at regular time intervals such that the evolution of grain size, grain coordination and grain shape can be evaluated. Dynamic grain growth rate, $\dot{d}_{\text{dyn}}$, was calculated according to the following relation (after Seidensticker and Mayo, 1998a):

$$\dot{d}_{\text{dyn}} = (d_{\text{total}} - d_{\text{static}})/t_{\text{total}} \tag{8}$$

where d_{total} is the grain size resulting from both static and dynamic contributions to grain growth, and d_{static} is the statically grown grain size over a similar period of time, t_{total}.

A single starting microstructure has been used for all simulations. It was made artificially, contains 1500 grains, and is single phased with zero porosity (see Fig. 4). The starting microstructure has close to lognormal grain size distribution and normal grain coordination number distributions (see Fig. 4b–c), similar to our forsterite microstructure (McDonnell et al., 1999; Kellermann Slotemaker et al., 2004). The microstructure is similar to microstructures commonly observed in natural rocks (e.g. Ranalli, 1984; Michibayashi, 1993; Dijkstra, 2001) and synthetically prepared materials (Karato et al., 1986; Rabinovich and Trifonov, 1996; Bergmann et al., 1998; Fayad et al., 1999; Ter Heege et al., 2005; Zhilyaev et al., 2005).

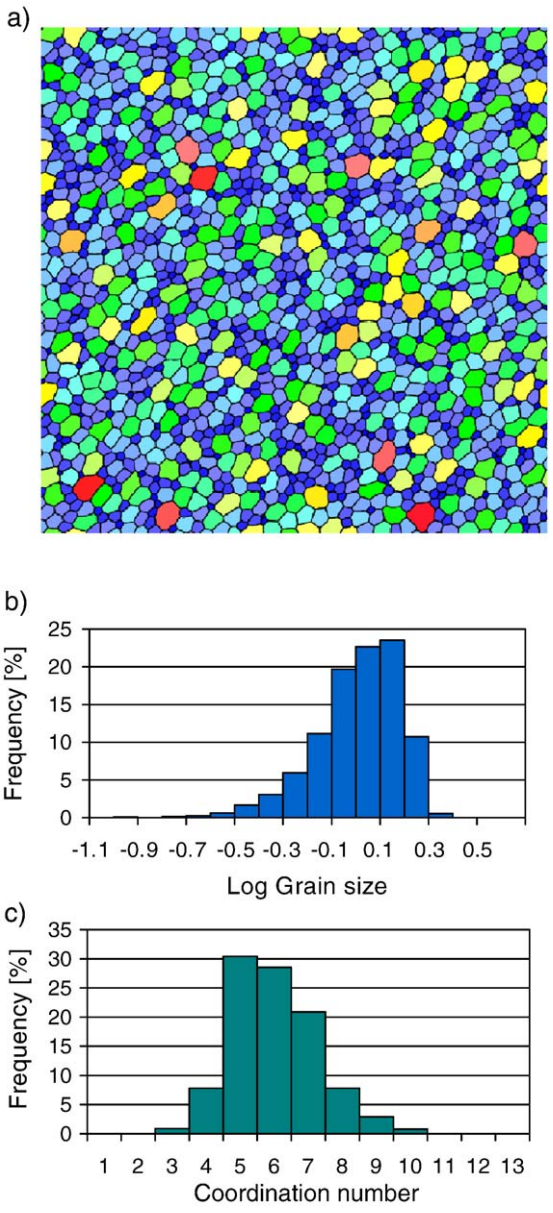

Fig. 4. (a) Starting microstructure used for all simulations. Color-coding represents grain size dependent viscosity variation. (b) Starting grain size distribution, showing a close to log-normal shape. (c) Starting coordination number distribution of approximate normal shape (cf. Fayad et al., 1999).

2.2. Simulations

As described above, simultaneous activity of GBM and deformation is modeled by iteratively combining small time and shear strain steps of each process respectively. Time is defined as the number of computational GBM *stages* that have elapsed. A time step has a prescribed number of GBM *stages* and is followed by a shear strain step with a preset size. Shear strain rate is then calculated as the ratio of shear strain step-size (dimensionless) over GBM time step-size (i.e. no. of *stages*) resulting in a unit of 1/stage. The GBM stage-unit used in the modeling could be converted to an absolute amount of time if constraints are available for the grain boundary mobility of the relevant material. Two simulation types (A and B) of combined deformation and GBM were performed:

Type A: We used *elle_manuel* for small steps of *homogeneous* deformation and *elle_gg* for small time-steps of GBM. In total 16 constant shear strain rate simulations were done up to a shear strain of 2, where shear strain rate was varied over 2 orders of magnitude.

Type B: We used *basil* for small steps of *GSS* creep and again *elle_gg* for small steps of GBM. 7 constant shear strain rate simulations were performed up to a shear strain (γ) of 2, with strain rate being varied one order of magnitude.

GBM time-step-size and shear strain step-size both can change the strain rate, but the smaller the time step the more closely truly contemporaneous activity of GBM and deformation is simulated, i.e. smaller time steps give higher resolution. Thus, to investigate grain growth behaviour at varying strain rates, it is most practical to only vary strain step-size and keep the time-step-size constant at a small value, maintaining a constantly high resolution. On the other hand, at constant strain rate a larger GBM time-step allows a larger deformation-step size, giving lower computation time. In about half of all simulations, we used the smallest possible time step size of 1 *stage*, but for

Table 1
List of all simulations and specific preset test-conditions

Test no.[a]	Simulation type[b]	Shear strain-step-size	GBM time-step-size (stages)	Shear strain rate (1/stage)	GBM speed-up factor
test33	A	1.0E−04	1	1.0E−04	0.3
test16	A	2.0E−04	1	2.0E−04	0.3
test19	A	4.0E−04	1	4.0E−04	0.3
test17	A	1.0E−03	1	1.0E−03	0.3
test15	A	2.0E−03	1	2.0E−03	0.3
test20	A	4.0E−03	1	4.0E−03	0.3
test18	A	1.0E−02	1	1.0E−02	0.3
test14	A	2.0E−02	1	2.0E−02	0.3
test34	A	5.0E−04	5	1.0E−04	1
test32	A	1.0E−03	5	2.0E−04	1
test31	A	2.0E−03	5	4.0E−04	1
test30	A	5.0E−03	5	1.0E−03	1
test29	A	1.0E−02	5	2.0E−03	1
test13	A	2.0E−02	5	4.0E−03	1
test25	A	5.0E−02	5	1.0E−02	1
test27	A	1.0E−01	5	2.0E−02	1
test23	B	4.0E−03	1	4.0E−03	0.3
test21	B	1.0E−02	1	1.0E−02	0.3
test22	B	2.0E−02	1	2.0E−02	0.3
test28	B	1.0E−02	5	2.0E−03	1
test11	B	2.0E−02	5	4.0E−03	1
test24	B	5.0E−02	5	1.0E−02	1
test26	B	1.0E−01	5	2.0E−02	1

[a] Note that each test number refers to both a combined GBM plus deformation test and a complementary single GBM test. All tests started with the same microstructure.
[b] A = homogeneous 'geometrical' deformation; B = heterogeneous GSS deformation.

practical (calculation-time) reasons the other half was done using a time step size of 5 *stages*. This also gave us the chance to check how sensitive the simulations were to a (5-fold) decrease in resolution. Furthermore, to detect the presence of possible large statistical uncertainties caused by a significant decrease in number of grains over long time periods (when imposing slow strain rates), we also varied the speed_up parameter in (5), setting its value to 1 or 0.3. This resulted in two combinations of preset test parameters for both type A and B simulations. We will refer to them as respectively the '5&1' and the '1&0.3' combination, where the first number refers to the GBM time step size (5 or 1) and the second number to the speed_up value (1 or 0.3). In addition, complementary static grain growth tests were done for each combined GBM + deformation simulation over similar periods of time, to be able to compare grain growth behaviour with and without contemporaneous deformation. A complete list of all simulations and specific preset conditions is given in Table 1. In the following, we will refer to a combined GBM-deformation simulation as 'testXX-dyn' and to a complementary static grain growth simulation as 'testXX-st'.

3. Results

3.1. Normal grain growth

A representative example of grain growth (test15-st) produced when only GBM is allowed to occur is shown in Fig. 5a. To show that this and other simulations produced realistic static grain growth kinetics, we used

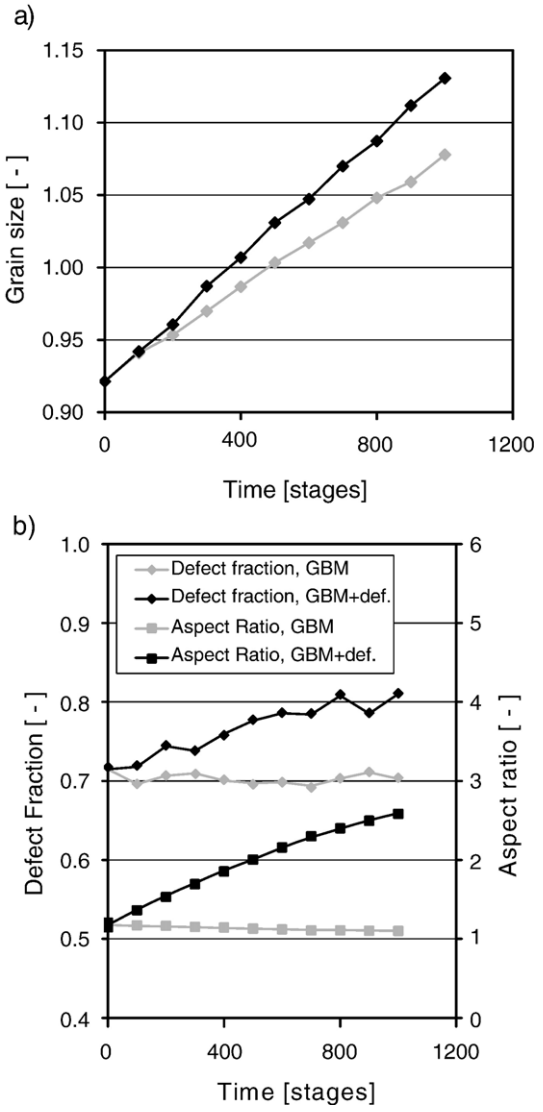

Fig. 5. (a) Increase in grain size (i.e. average equivalent circular diameter) resulting from simulation test15-st for static grain growth (gray symbols and line) and for the combined deformation plus GBM simulation (black symbols and line). (b) Evolution of defect fraction and aspect ratio for test15. Defect fraction and aspect ratio remain more or less constant at their starting values during the static grain growth simulation, while they show gradual but significant increase for the combined deformation plus GBM simulation.

the conventional grain growth law (after Burke and Turnbull, 1952; Atkinson, 1988; Evans et al., 2001) given by:

$$(d_{\text{static}})^n - (d_0)^n = k \cdot t \quad (8)$$

where d_0 is the initial grain size, t is time, n is the grain growth exponent (typically varying between 2 and 5; Evans et al., 2001), and k is a temperature-dependent rate constant. Using linear regression analysis in $(d_{\text{static}})^n - (d_0)^n$ versus t space, and taking k as a constant, a best fit of the growth data of test15-st to Eq. (8) gives $n=2.0$, with a correlation coefficient, R^2, of 0.9990. Considering all static grain growth tests with a minimum duration of 500 *stages*, we found the average best-fit n-value is 2.3 ± 0.3. More pronounced variation occurs in shorter duration tests, i.e. for $t<500$ *stages*. Thus, following an initial transient stage, static grain growth conforms well to the theoretical 'exponential' law (Eq. (8)). Furthermore, defect fraction and aspect ratio are both more or less constant during normal grain growth, as shown by characteristic plots of both parameters versus time for test15-st in Fig. 5b. For a quantitative overview of the microstructural parameters for all tests see Table 2. In general, defect fraction only slightly varies between 0.67 and 0.72, with an exception for a few tests with a *duration* ≥ 5000 *stages*, where its value can drop as low as 0.54 (Table 2). Microstructural evolution during static grain growth (test15-st) is shown in Fig. 6a–e at time intervals of 250 *stages*.

3.2. Combined GBM and homogeneous deformation

3.2.1. Dynamic grain growth and evolution of grain geometry

In the case of combined GBM and homogeneous deformation, a component of extra 'dynamic' grain growth is observed compared to the static grain growth curve. This is well illustrated by the results of test15-dyn (Fig. 5a). Both defect fraction and aspect ratio significantly increase with time (and strain) compared to the semi-constant values measured during normal grain growth (Figs. 5b and 6f–j). Increase of defect fraction (from an initial value of 0.71) is gradual and reaches values up to 0.81 at the end of the runs, where $\gamma=2$. This microstructural evolution is consistently found to be the same in all of the combined deformation plus GBM tests. Final defect fraction values of all simulations are summarized in Table 2.

Table 2
Quantitative overview of main simulation results for all tests

Test no.	Duration (stages)	Final values GBM test (static grain growth)			Final values GBM+def test (dynamic grain growth)						Average DGG-rate (1/stage)
		No. of grains	Average grain size	Defect fraction	Shear strain	No. of grains	Average grain size	Defect fraction	Aspect ratio	DGG-fraction (%)	
test33	20000	213	2.44	0.54	2.0	199	2.53	0.75	2.05	5.26	$8.03*10^{-7}$
test16	10000	355	1.89	0.69	2.0	319	2.00	0.72	2.12	9.66	$4.61*10^{-6}$
test19	5000	559	1.51	0.72	2.0	496	1.60	0.81	2.24	13.66	$1.14*10^{-5}$
test17	2000	849	1.22	0.68	2.0	770	1.29	0.80	2.42	16.81	$2.61*10^{-5}$
test15	1000	1096	1.08	0.70	2.0	996	1.13	0.81	2.59	25.23	$4.97*10^{-5}$
test20	500	1265	1.00	0.70	2.0	1184	1.04	0.80	2.97	29.17	$8.33*10^{-5}$
test18	200	1401	0.95	0.71	2.0	1333	0.98	0.80	3.69	42.87	$1.22*10^{-4}$
test14	100	1438	0.94	0.70	2.0	1397	0.95	0.77	4.45	41.09	$1.57*10^{-4}$
test34	20000	84	3.89	0.71	2.0	76	4.09	0.68	1.95	6.30	$4.73*10^{-6}$
test32	10000	159	2.83	0.62	2.0	140	3.02	0.68	2.02	8.88	$4.19*10^{-6}$
test31	5000	244	2.28	0.59	2.0	235	2.33	0.77	2.05	3.08	$4.92*10^{-6}$
test30	2000	468	1.65	0.71	2.0	424	1.73	0.81	2.18	10.29	$2.90*10^{-5}$
test29	1000	694	1.35	0.68	2.0	615	1.44	0.80	2.32	16.30	$5.05*10^{-5}$
test13	500	922	1.18	0.70	2.0	841	1.23	0.82	2.44	17.89	$1.05*10^{-4}$
test25	200	1210	1.03	0.70	2.0	1117	1.07	0.80	2.73	28.60	$2.23*10^{-4}$
test27	100	1341	0.97	0.71	2.0	1253	1.01	0.81	3.19	38.78	$3.63*10^{-4}$
test23	450	1284	1.00	0.70	1.8	1204	1.03	0.82	2.84	30.41	$8.03*10^{-5}$
test21	160	1412	0.95	0.70	1.6	1376	0.96	0.79	3.27	30.39	$7.76*10^{-5}$
test22	90	1449	0.94	0.70	1.8	1407	0.95	0.79	3.94	46.35	$1.36*10^{-4}$
test28	1000	694	1.35	0.68	2.0	585	1.48	0.80	2.12	21.81	$7.65*10^{-5}$
test11	500	922	1.18	0.70	2.0	798	1.26	0.83	2.30	25.75	$1.56*10^{-4}$
test24	200	1210	1.03	0.70	2.0	1161	1.05	0.78	2.73	17.02	$2.23*10^{-4}$
test26	100	1341	0.97	0.71	2.0	1277	1.00	0.81	3.21	31.24	$2.51*10^{-4}$

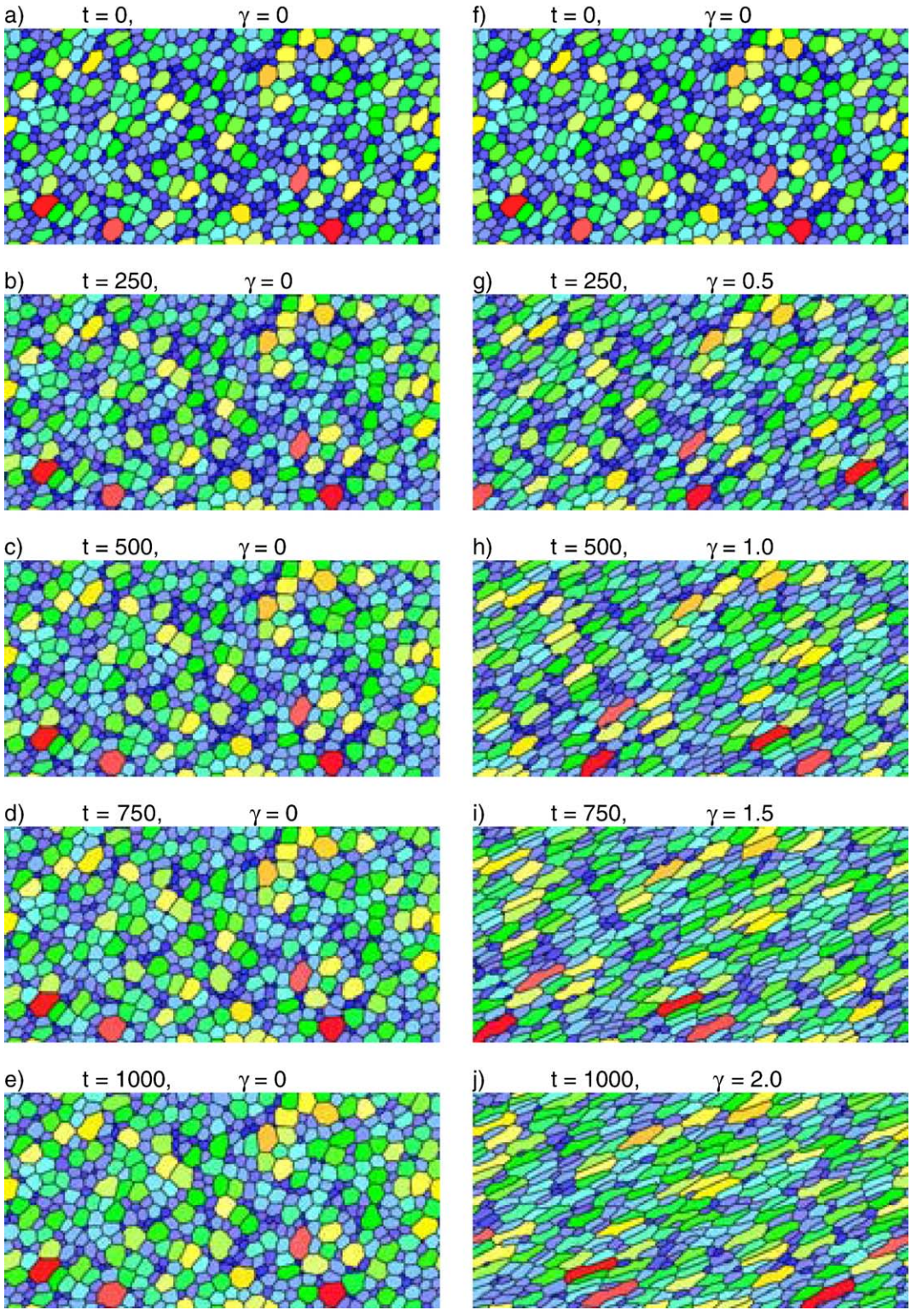

Fig. 6. Microstructural evolution during test15 of (a)–(e) the static grain growth simulation and (f)–(j) the combined deformation plus GBM simulation.

3.2.2. Dynamic grain growth rate and effect of strain rate

The rate of DGG is evaluated for all simulations using relation (2). The normalized DGG rate shows more or less constant behaviour with ongoing strain/time at constant strain rate after an initial period of transient DGG rates (Fig. 7). For most simulations, a continuous slight decrease in DGG rate is observed at shear strains above 1.0. This is best seen in the higher strain rate tests. However, this decrease of normalized DGG-rate with time is small compared to the increase in DDG rate with increasing strain rate (cf. test14-dyn to test33-dyn; Fig. 7). To get a better picture of how DGG-rate increases with strain rate, we calculated the average normalized DGG-rate for each test, using only data for $\gamma = 1$ and higher, i.e. when the dynamic grain growth rate is more or less constant. The increase of the averaged normalized DGG rate with strain rate is shown in Fig. 8. The two different curves in Fig. 8 correspond to the two different combinations of 'GBM time-step size' and 'speed_up'-values (see Table 1). As long as λ and k' in Eqs. (1)–(3) are constant, a linear relation with a slope of 1 can be expected between DGG rate and natural strain rate (in the log–log space of Fig. 8). This appears to be the case for intermediate values of strain rate, where both types of GBM+deformation combinations overlap. At higher strain rates, data lie below this linear trend, implying decreasing values for λ (cf. Eq. (2)). This is more pronounced for the 1&0.3 combination. Also at low strain values, the data do not follow the linear trend of the intermediate strain rates, the 5&1.0 value being anomalously different.

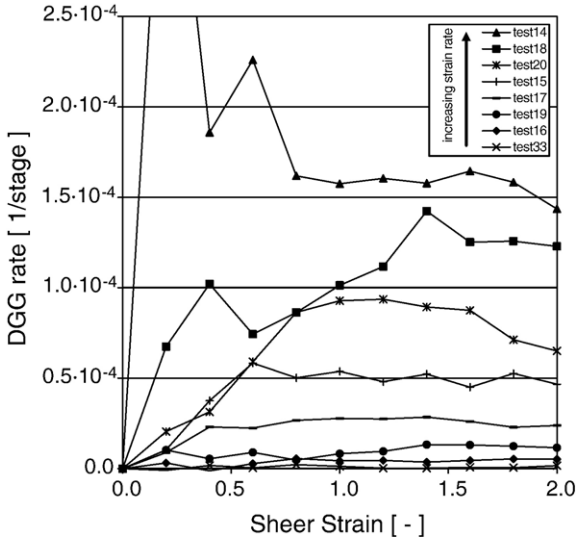

Fig. 7. Evolution of normalized DGG rate with strain for all Type A, 1&0.3-combination tests.

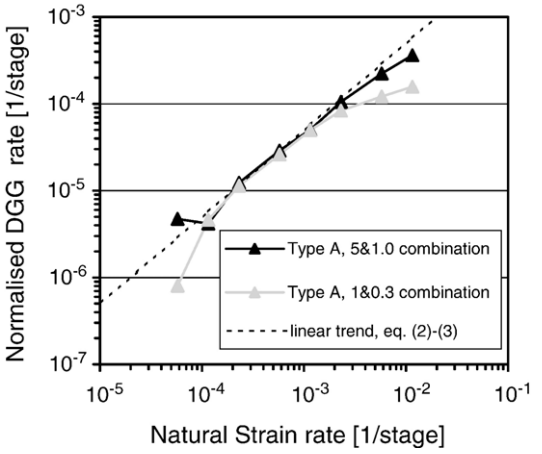

Fig. 8. Log-scale plot of average normalized DGG rate versus natural strain rate for all Type A, i.e. homogeneous deformation plus GBM, combined tests. A linear trend line is shown for Eq. (2), if λ and k' in (3) are constant.

Fig. 9 shows the final average aspect ratio of the grains at $\gamma = 2$ as a function of strain rate. We observe more flattening (increase in aspect ratio) when the strain rate is higher. Moreover, Fig. 9 shows that for high resolution but low speed_up (1&0.3) there is significantly more increase in aspect ratio, especially at the highest strain rates, compared to lower resolution but higher speed_up (5&1.0).

The evolution of defect fraction with strain, as a function of strain rate, is shown in Fig. 10. There is some scatter in defect fraction evolution with varying strain rate, but no systematic dependence on strain rate emerges from the data (Fig. 10a,c). At shear strains above ~1.4, a

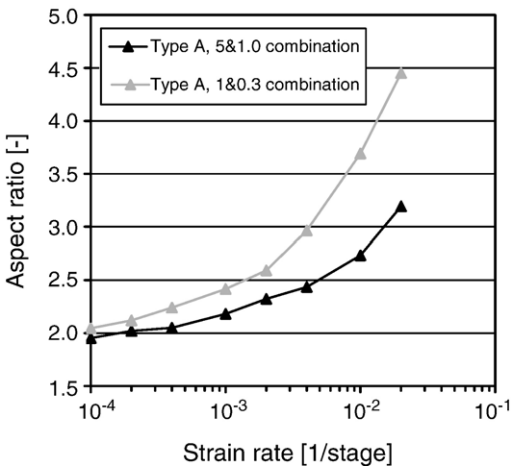

Fig. 9. Dependence of aspect ratio on strain rate for all Type A tests, i.e. homogeneous plus GBM. Aspect ratios taken at shear strain of 2.

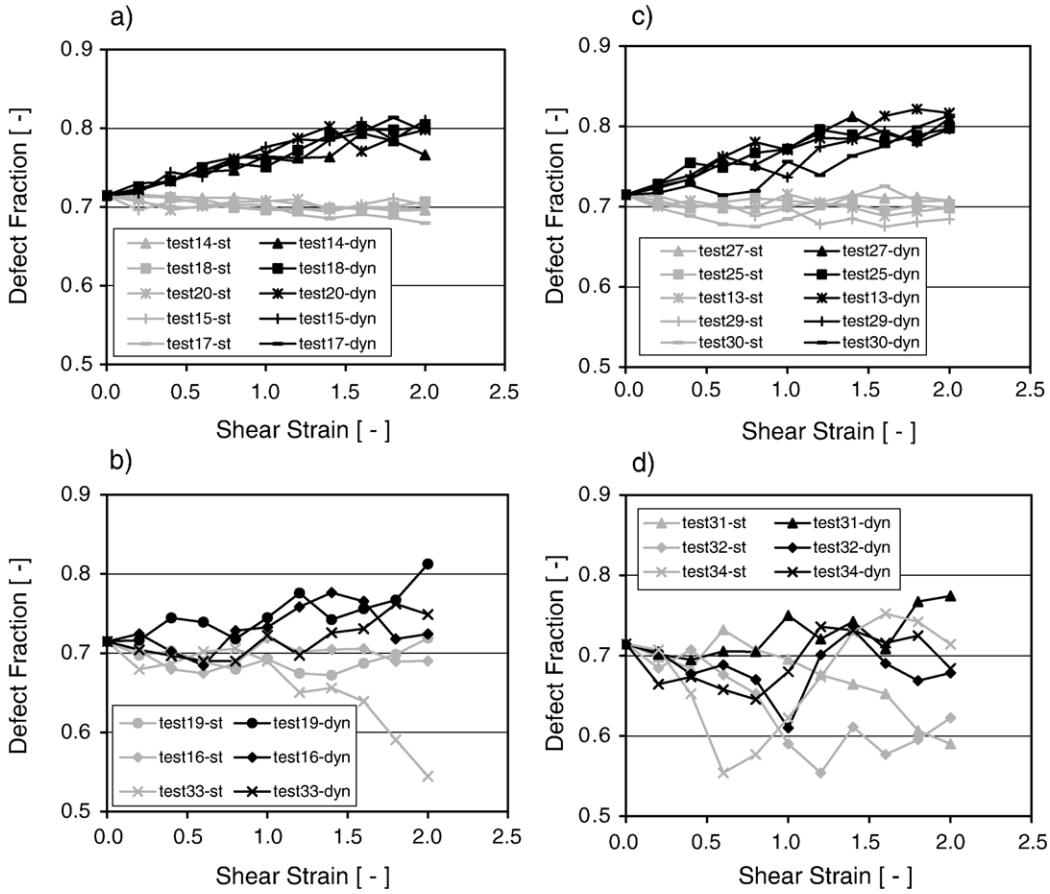

Fig. 10. Evolution of defect fraction, X_d, with strain for all Type A tests; (a) 1&0.3-combination tests with shear strain rate $>4.0\times10^{-4}$, (b) 1&0.3-combination tests with shear strain rate $\leq4.0\times10^{-4}$, (c) 5&1.0-combination tests with shear strain rate $>4.0\times10^{-4}$, (d) 5&1.0-combination tests with shear strain rate $\leq4.0\times10^{-4}$.

constant value for the defect fraction is approached within the range 0.76–0.81. While trends are clearly defined at fast strain rates, defect fractions for both single GBM and GBM plus deformation irregularly vary and reach lower values as a function of strain at low shear strain rates, i.e. $\leq4.0\times10^{-4}$ (Fig. 10b,d and Table 2).

3.3. Combined GBM and GSS deformation

3.3.1. Dynamic grain growth and evolution of grain geometry

Test28-dyn (Table 2)) is a representative example of combined GBM and GSS deformation at an intermediate strain rate. In this test, we observed more DGG during GSS deformation compared to homogeneous deformation (test29-dyn) (Fig. 11a). The evolution of defect fraction is similar to that in the homogeneous case, but less increase in aspect ratio is observed (Fig. 11b). Qualitatively, small grains in the distribution seem to develop a stronger grain shape preferred orientation than larger grains, but with decreasing grain size at the final shrinking stages, this stronger aspect ratio diminishes again (Fig. 12).

3.3.2. Dynamic grain growth rate and effect of strain rate

Fig. 13 shows the dependence of DGG rate on strain rate for all GSS deformation plus GBM combined simulations. For the type B 5&1.0-combination, the usual increasing trend in DGG rate with increasing strain rate is observed, but at higher strain rates there is a strong deviation from the linear trend expected if λ (and k') is constant (Fig. 13). All type B 1&0.3 simulations show lower DGG rates and no real trend can be observed. This is partly due to the fact that the range in strain rate is small and restricted to the higher values: because of rapidly increasing calculation times it became impractical to perform type B simulations at lower strain rates. It is only at the lowest two applied strain rates for the type B 5&1.0-combination, i.e.

test28-dyn and test11-dyn, that we observe a higher DGG rate when compared to the equivalent homogeneous deformation tests. All remaining GSS deformation tests show a lower or equal DGG rate (Fig. 13), suggesting lower or equal λ-values. Similarly, aspect ratio analysis only shows significantly lower values for test28-dyn and test11-dyn (Fig. 14). The microstructure developed in the higher strain rate tests (test21-dyn to test24-dyn and test26-dyn) shows that small grains locally develop unrealistically large aspect ratios. Furthermore, only a few small grains seem to be able to shrink enough for them to regain a more or less equidimensional shape (Fig. 15). This delayed their final disappearance.

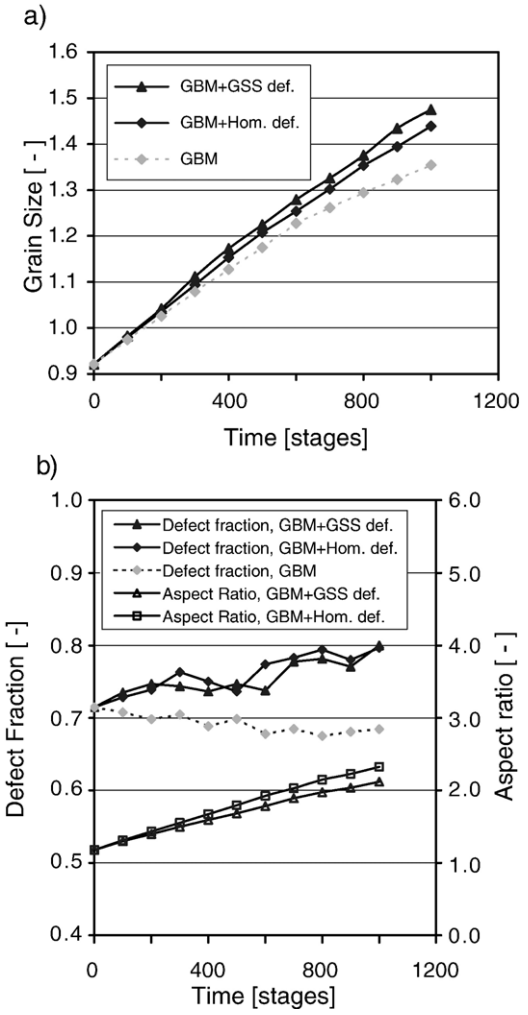

Fig. 11. (a) Evolution of grain size with time for static grain growth (GBM) (dotted line and diamond gray symbols, test28–29), combined GBM plus homogeneous deformation (continuous line and diamond black symbols, test29), and combined GBM plus GSS deformation (continuous line and triangle symbols, test28). Note enhanced grain growth in the GBM plus GSS deformation run (test29) compared with the other types of simulation. (b) Evolution of defect fraction and aspect ratio for GBM plus deformation (homogeneous or GSS); both show gradual but significant increase.

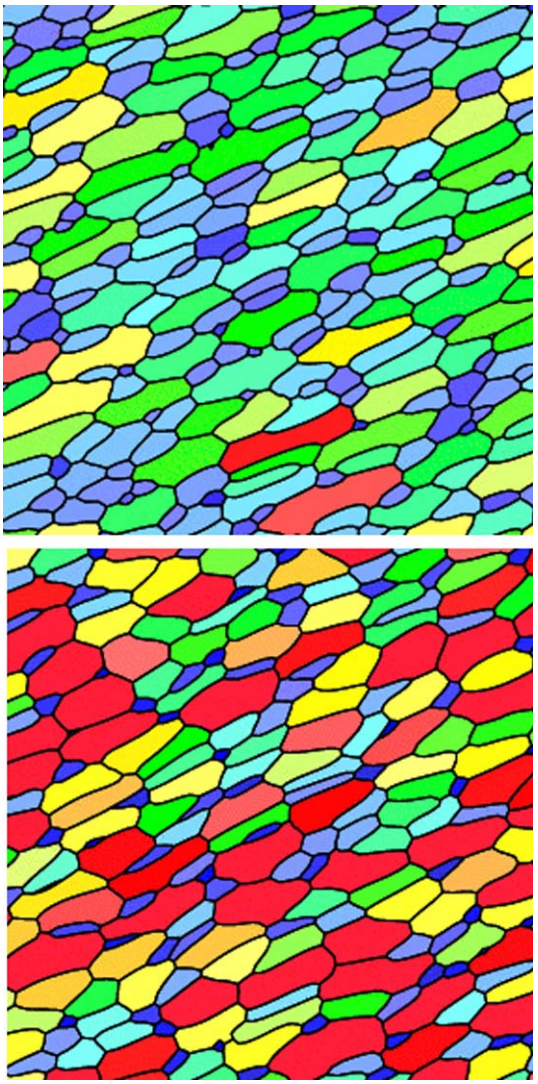

Fig. 12. Microstructures (lower left quarter of modeled square cell) of test13 (upper image) and test11 (lower image) at a shear strain of 2. Test13 is a homogenous deformation plus GBM combined simulation showing a clear homogenous flattening of all (large and small) grains. Test11 is the equivalent GSS deformation plus GBM combined simulation showing that, in comparison to test13, larger grains are less flattened, while smaller grains have higher aspect ratios. Note the few smallest grains that show a more or less equidimensional shape.

4. Discussion

4.1. Mechanism of modeled DGG

Using 2D microstructural modeling to combine simple homogeneous (or inhomogeneous GSS) deformation and

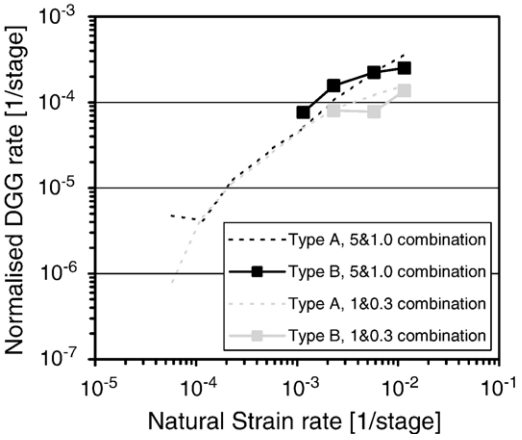

Fig. 13. Log-scale plot of average normalized DGG rate versus natural strain rate for all type B, i.e. GSS deformation plus GBM, combined tests. Type A tests are also shown as lines without symbols for comparison (taken from Fig. 8).

GBM, we observed a component of grain growth not seen under static conditions. In other words, we produced strain induced (dynamic) grain growth. In association with the dynamic grain growth, a systematic increase in cellular defect fraction, X_d (3), as a function of strain was observed (Figs. 5b and 10). A change in defect fraction, and hence in grain topology, together with a change in average grain size, implies that extra grain neighbor switching must have taken place. Our modeling thereby demonstrates the general validity of the hypothesis that extra neighbor switching induced by deformation causes an increase in cellular defect fraction, which in turn leads to enhanced grain growth. Our modeling involved

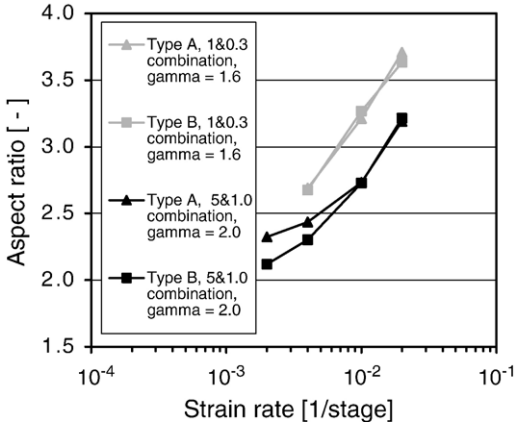

Fig. 14. Dependence of aspect ratio on strain rate for all type B, i.e. homogeneous plus GBM, combined tests at constant shear strain of 1.6 for the 1&0.3 combination and at a shear strain of 2 for the 5&1.0 combination. Equivalent type A values are also included for comparison.

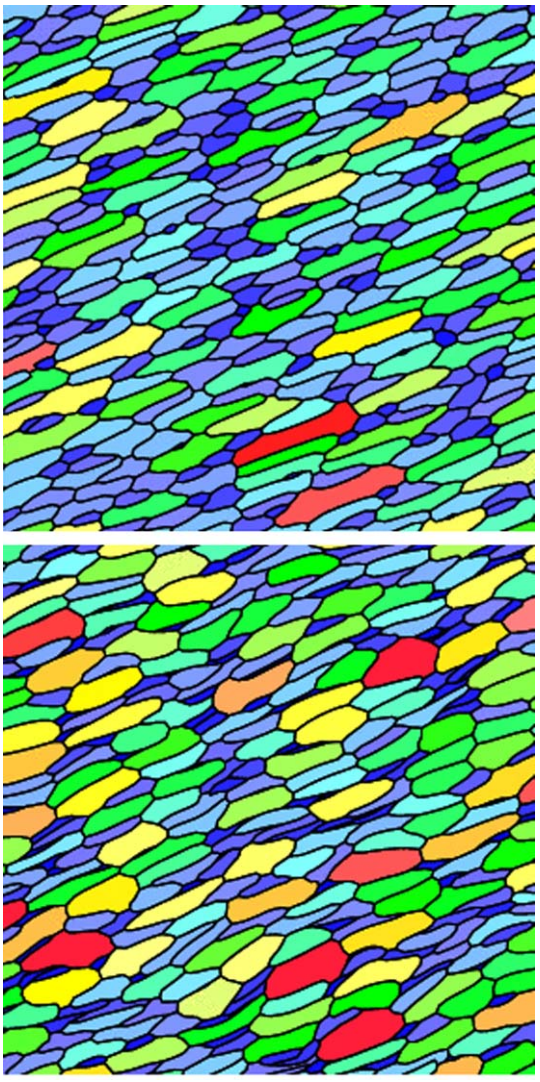

Fig. 15. Microstructures (lower left quarter of modeled square cell) of test27 (upper image) and test26 (lower image) at a shear strain of 2 and higher strain rate than in Fig. 12. Test27 is a homogenous deformation plus GBM combined simulation showing a clear homogenous flattening of all (large and small) grains. Test26 is the equivalent GSS deformation plus GBM combined simulation showing that, in comparison to test27, larger grains are less flattened, while smaller grains have higher aspect ratios. Moreover differences in aspect ratio between large and small grains have become more pronounced, such that now also most of the smallest grains show significant flattening.

homogeneous or inhomogeneous straining of grains rather than GBS plus accommodating diffusion creep (cf. Fig. 2). Grain neighbor switching in our deforming aggregates with distributed grain size and coordination number can be envisaged as depicted in Fig. 16. Here it is schematically shown how extra deformation-induced neighbor switching can take place compared to static GBM. Compared to one switching event in Fig. 1b, two

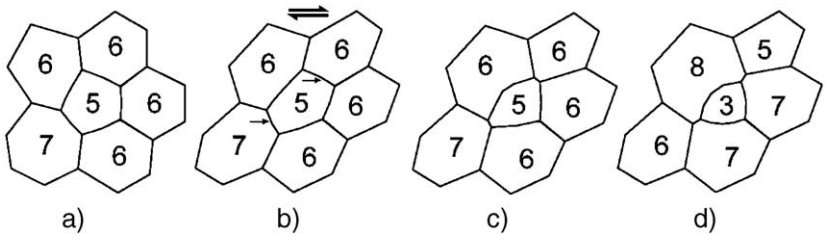

Fig. 16. Schematic drawing of geometrical strain plus GBM induced grain neighbor switching in an aggregate with distributed grain size and coordination number. (a) Initial microstructure similar to Fig. 1a, $X_d = 2/6 = 0.33$. (b) Sheared microstructure, small arrows indicate grain boundary segments of the 5-sided grain, which are bounded by distorted triple junctions, i.e. ≠120 angles, $X_d = 2/6 = 0.33$. (c) The unstable triple junctions have moved toward each other via GBM to regain a stable geometry, $X_d = 2/6 = 0.3$. (d) Ongoing GBM has led to 2 switching reactions and the 5-sided grain has become 3-sided. Only one 6-sided grain remains, giving a defect fraction of 0.83 in this particular microstructure.

switching events occurred in Fig. 16d, leading to a higher defect fraction and more rapidly shrinking small grains. For example, compare the 3-sided grain in Fig. 16d with the larger 4-sided grain in Fig. 1b.

Any 2D grain neighbor switching event is preceded by a stage in which the grain boundaries involved form a quadruple point. There are various ways to develop a quadruple point. One scenario, proposed by Bons and Urai (1992; their Fig. 10), showed how homogeneous flattening of a group of 4 equally-sized ideal hexagonal grains (Fig. 2a) can result in (extra) surface-energy-driven GBM, leading to strain-induced neighbor switching without grain growth. In their approach, the evolution of grain boundary geometries up to ca. 40% shortening (0.5 natural strain) results in an unstable stage when two triple points merge into a quadruple point, where the boundaries intersect at 60° and 120° angles. In this evolution, grains develop an elongated shape (aspect ratio >1). Pure grain boundary or lattice diffusion (Coble or Nabarro-Herring) creep can produce a similar quadruple point. These diffusion mechanisms change the shape of the grains, as is the case in the Bons and Urai (1992) scenario, but do not disturb the 120° equilibrium angles at triple points. Although the theories behind conventional Coble and Nabarro-Herring GSS creep do not explicitly include any grain switching, such microstructural modification is inevitable for the 4 grain-aggregate with ideal hexagonal grains as used by Bons and Urai (1992), as can be seen in Fig. 2. Ashby and Verrall (1973) explicitly incorporate neighbor switching in a model for diffusion-accommodated GBS and also predict a quadruple point stage at ca. 40% shortening (cf. Bons and Urai, 1992). In contrast to the above scenarios, in their model all boundaries are now at 90° angles, and no elongated grain shape develops. Further, Ashby and Verrall's model presumes a completely different flow pattern on the grain scale, i.e. less volume displaced per unit strain and a shorter length of diffusion pathways compared to conventional GSS creep. Irrespective of how a quadruple point develops, the geometry will be unstable and will be modified by a subsequent stage of GBM to re-equilibrate grain boundaries. As a result, a single indistinguishable grain boundary geometry develops, with equal-sized and equidimensional hexagonal grains. We suggest it is reasonable to assume that all types of deformation-related neighbor switching lead to similar changes in topology of aggregates with distributed grain size and distributed coordination number (in contrast to an idealized honeycomb network). This may affect two measurable microstructural parameters: (1) it can increase the defect fraction, following Sherwood and Hamilton (1992), and (2) it can enhance the grain growth. Both of these effects are observed in all our tests. Two important caveats to the above must be dealt with. First, the homogeneous flattening as modeled in the present study lacks a true physical basis in terms of a specific deformation mechanism. Thus, process rates as seen in the modeling, for instance the number of grain switching events per strain or time increment, might be very different from nature. However, from the above it appears that flattening plus GBM, as applied in simulations (Bons and Urai, 1992), will produce neighbor switching at roughly the same strain as predicted for theoretically based diffusion-accommodated GBS or conventional GSS creep. The amount of strain necessary to induce a neighbor switching, obviously, controls the number of switching events per time unit (at a certain strain rate) and thus most likely effects the resulting dynamic grain growth rate. We therefore do not expect large differences in dynamic grain growth rate to be produced by the present modeling, in experiments, or in nature. A second point is that the present modeling produces a strong grain shape preferred orientation with increasing strain. However, in real materials and natural rocks deformed by dominant GSS creep, a large component of GBS is frequently inferred and grain-shapes are more or less equidimensional even if large strains were

reached. This marked difference between the present modeling and nature does result in dissimilar (dynamic) grain growth rates, which will be discussed further below.

4.2. Microstructural evolution and strain rate effects

Together with a gradual increase in defect fraction, we also observed an increase in aspect ratio with strain (Fig. 5b). Bons and Urai (1992) performed similar combined GBM plus deformation simulations to those of our study and observed that GBM tends to impede the increase in aspect ratio when compared to deformation without GBM. They further concluded that the presence of a strong aspect ratio slows down grain growth. This conclusion was based on the comparison of results from two modeling runs with different starting microstructures. In one run, an initial microstructure was homogeneously flattened first, before static grain growth was allowed. In the other run, the same initial microstructure was allowed to grow without prior deformation. Our approach was different, since grain growth and flattening occurred (quasi) simultaneously. Nevertheless, we confirm the conclusion of Bons and Urai (1992) as shown by our observation of a small but systematic decrease in DGG rate with strain (i.e. flattening) at constant strain rate (see Fig. 7), together with a prominent decelerating increase in DGG-rate with increasing strain rate (see Fig. 8). This correlates well with a strain- and strain rate-dependent increase of aspect ratio (see Figs. 6 and 9). In our simulations, the retarding effect of aspect ratio formation on grain growth does not result in less net grain growth compared to the static tests. This is because of the enhancing effect of deformation on grain growth related to neighbor switching, which probably dominates the impeding effect of aspect ratio increase.

The divergence between the 5&1.0 and 1&0.3 combinations in Fig. 8 at higher shear strain rates (2×10^{-3}–2×10^{-2}) appears strongly related to stronger aspect ratio formation at a lower speed_up -value (or GBM mobility), as shown in Fig. 9. At lower intermediate shear strain rates (4×10^{-4}–2×10^{-3}), both combinations overlap and the DGG rate parameter λ in relations (1)–(3) is more or less constant (Fig. 8). In addition, we found a very consistent increase in defect fraction, X_d (3), which approaches a constant level around 0.81 at these strain rates (see Fig. 10a,c). In other words, both rate parameter λ and defect fraction remain constant with increasing (intermediate) strain rate. Moreover, the decrease in λ at the lowest shear strain rates (1×10^{-4}–4×10^{-4}) correlates well with the decreasing trend in defect fraction for static grain growth tests and with the greater variability and smaller increase in defect fraction for combined GBM plus deformation tests (Fig. 10b,d). This supports the hypothesis that λ is strongly related to defect fraction, X_d, as in Eq. (3). At lower strain rates, the increased variability in defect fraction is probably an artifact of the decrease in number of grains after long periods of time. This causes statistical inconsistencies in the distributions in grain size and coordination number of the strongly coarsened modeled aggregate. This must also have triggered the anomalous high DGG-rate at the lowest stain rate for the 5&1.0 combination (test34-dyn), as this microstructure experienced the greatest amount of grain growth of all the simulations; in fact only 76 grains remained from the 1500 grains at the start (see also Table 2).

4.3. The effect of GSS deformation

In order to obtain a crude impression of the effect of GSS deformation, we invoked viscosity decrease with decreasing grain size in our model, so that smaller grains were more easily deformed and flattened than larger grains (Fig. 12). Compared to grains undergoing homogeneous deformation, this resulted in a more heterogeneous evolution of aspect ratio and grain shape preferred orientation, which can explain higher DGG rates at slower strain rates and lower DGG rates at higher strain rates. At intermediate strain rates, the local strain heterogeneities between larger and smaller grains result into a lower overall aspect ratio (test28-dyn and test11-dyn, Fig. 14) and thus higher DGG rates compared to homogeneous deformation under the same conditions. The higher strain rates and/or lower speed_up values in all other GSS tests result in similar aspect ratios compared to homogenous deformation. Nevertheless, the strain heterogeneities are perhaps even more prominent in these tests (Fig. 15) and we propose that, in this case, GBM of the now strongly flattened smallest grain size fraction cannot keep up with the deformation (see also Bate, 2001). This may impede final shrinkage and may prevent disappearance of these smallest grains (Fig. 15), leading to lower DGG rates compared to homogeneous deformation. Advances in modeling techniques eventually will allow more physically based simulation of GSS creep, possibly including accommodation by GBS and grain rotation (e.g. Ford et al., 2002) to be incorporated in ELLE. This will limit the formation of a strong aspect ratio and its significant effect on DGG behaviour at high strain rates and would make the results better applicable to interpreting the behaviour of natural rocks and superplastically deformed materials. Our goal in the present study was only to investigate whether GBM plus geometrical (in)homogeneous deformation could induce

extra neighbor switching, resulting in a higher defect fraction and in enhanced grain growth.

As noted above, an increase in aspect ratio is found to have a strong decelerating effect on the rate of dynamic grain growth. We further emphasize that in this study we did not include dislocation activity, related grain size reduction, formation of interconnected weak layers, or other development of organized strain heterogeneities. In case these processes are active, an increasing dynamic grain growth rate with increasing strain rate will be difficult to interpret, in particular because faster strain rate generally gives higher stresses resulting in smaller (!) recrystallized grain sizes. In the following sections we will further elaborate on the relevance of the model results for natural systems and experiments on real materials.

4.4. Comparison to existing models and experimental work

The various theoretical, modeling and experimental studies on DGG have indicated a range of values for the strain rate sensitivity of rate parameter λ in (1)–(3), from 0.13 (Seidensticker and Mayo, 1998a) up to ~ 1 (Wilkinson and Caceres, 1984). Seidensticker and Mayo (1998a) summarized DGG data on a wide range of metallic and ceramic materials tested within a large range of temperatures and found surprisingly consistent strain rate dependency. The compiled data of Seidensticker and Mayo (1998a) fall within a band of linear strain rate sensitivity λ with upper and lower limits of 0.04 and 1, respectively (average 0.13). A comparison of our data to the calibration by Seidensticker and Mayo (1998a) is shown in Fig. 17. Our simulation data for λ (Figs. 8, 11 and 17) vary between 0.07 and 0.01, and are positioned near the lower limit of the range for real materials of Seidensticker and Mayo (1998a). This first order agreement of the modeling results with experimental data on real materials gives confidence in the general validity of our conclusions. If anomalous aspect ratio development in future modeling can be reduced (see Section 4.3), DGG rate might very well reach the average λ of 0.13. At the highest strain rates, the experimental record shows incipient breakdown of the linear relationship due to a supposed deformation mechanism switch from superplasticity to dislocation creep (Wilkinson and Caceres, 1984). This nicely agrees with the lower DGG rate values predicted in this study at the highest strain rates. If such a mechanism switch is accompanied by an increase in aspect ratio formation, our modeling may provide a good approximation of this breakdown in the linear trend of natural strain rate vs. normalized DGG rate.

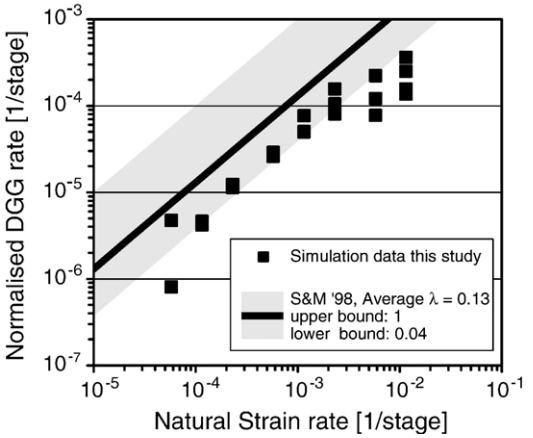

Fig. 17. Log-scale plot of average normalized DGG rate versus natural strain rate for all simulations of this study (of Figs. 6 and 13) compared to the average linear relationship calibrated by Seidensticker and Mayo (1998a,b) and the upper and lower bounds of this calibration.

The microstructural modeling study of Bate (2001) investigated GBM during deformation of uniform Zener-pinned aggregates and produced higher DGG rates and λ (0.4 to 0.5) than those from the compilation of Seidensticker and Mayo (1998a) or from our simulation runs. This suggests that if Zener-pinning could be introduced into our simulations, the component of dynamic grain growth may well be significantly larger. We aim to take this into account in future modeling, as our forsterite microstructures (Kellermann Slotemaker et al., 2004) also showed definite effects of grain boundary pinning. It is worth noting that the ELLE system has the potential to model non-uniform Zener-drag by introducing an unconnected distribution of discrete second phase grains into the microstructure, which would be even more realistic than the applied uniform Zener-drag by Bate (2001).

4.5. Relevance of the model results to natural rocks

The results of the ELLE 2D microstructural modeling suggest that analysis of the fraction of non-hexagonal grains in a deformed material represents a way to establish whether dynamic grain growth has occurred. Recognizing this process in natural rocks can be of great help in the interpretation of the rheological behaviour in a geodynamic context. In order to test and illustrate the potential of defect fraction analysis, we measured defect fractions in some natural calcite mylonites from the Helvetic Alps, Switzerland. The samples were selected from a suite of calcite rocks that show significant syndeformational grain growth, analyzed in detail by Herwegh et al. (2005). The

mylonites come from thrust planes in a nappe stack consisting of the Doldenhorn, Gellihorn and Wildhorn nappes. The initially fine-grained limestones were inferred to have been deformed at a strain rate of about 10^{-11} s^{-1} and a temperature between 250 and 379 °C. With increasing deformation temperature, the grain size and grain aspect ratio increases (Table 3, Fig. 18), while the crystallographic preferred orientation of calcite *c*-axes remains of similar strength. Rheological modeling using full grain size distributions and composite flow laws for GSS and grain size insensitive (GSI) creep (see Ter Heege et al., 2004) indicate an increase in the GSS component of the overall creep rate with increasing temperature (see Table 3). From the measurements and modeling, Herwegh et al. (2005) concluded that with increasing temperature (a) grain growth became the major microstructure modification process in the fine-grained rocks, and (b) enhanced mass transfer / diffusion processes occurred, rather than increased activity of dislocation mechanisms.

The same (2D) grain boundary maps as used by Herwegh et al. (2005) were taken to measure grain coordination numbers and to determine defect fractions (Table 3, Fig. 18). The defect fraction was found to be relatively low (~0.75) at low temperature, in samples dominantly deformed by GSI mechanisms. Given that these samples were highly strained, but show small grain sizes and low aspect ratios, competition between grain growth and grain size reduction must have kept the grains relatively small and close to equidimensional. This produced a microstructure that looks 'static', which is consistent with the low defect fraction. In contrast, the calcite mylonites deformed at higher temperature show high defect fractions (~0.9). The increase in defect fraction corresponds to the change in slope in the grain size vs. temperature and aspect ratio vs. temperature trends (Fig. 18). Following Herwegh et al. (2005), these microstructure modifications indicate an increased contribution of grain growth to the grain size stabilization process. Apparently, anisotropic grain growth becomes more prominent at higher temperature, related to a more pronounced contribution of GSS mechanisms to the overall creep. The higher defect fraction at higher temperature is fully consistent with this, suggesting grain neighbor switching played an important role in the deformation.

In summary, the increased component of syndeformational grain growth and the enhanced contribution of GSS creep mechanisms to the overall creep inferred by Herwegh et al. (2005) for the Helevetic limestones are

Table 3
Data overview natural calcite mylonites

Sample	Temp, T (°C)	$1/T$ (10^3/K)	Grain size (μm)	Aspect ratio	% GSS[a] (%)	Defect fraction
Ge-3	250	1.91	2.5	1.25	~0.3	0.76
Wi-16	317	1.69	7.0	1.56	~2.0	0.74
Do-8	345	1.62	10.7	1.47	93–100	0.78
Do-28	361	1.58	23.7	1.75	60–100	0.91
Jung-986	379	1.53	40.6	2.78	31–87	0.93

[a] %GSS indicates the relative contribution of GSS creep to the total. Calculation of %GSS depends on the character of the grain size distribution, chosen experimentally calibrated flow laws and assumptions regarding homogeneous stress or homogeneous strain rate through the aggregate (see Herwegh et al., 2005).

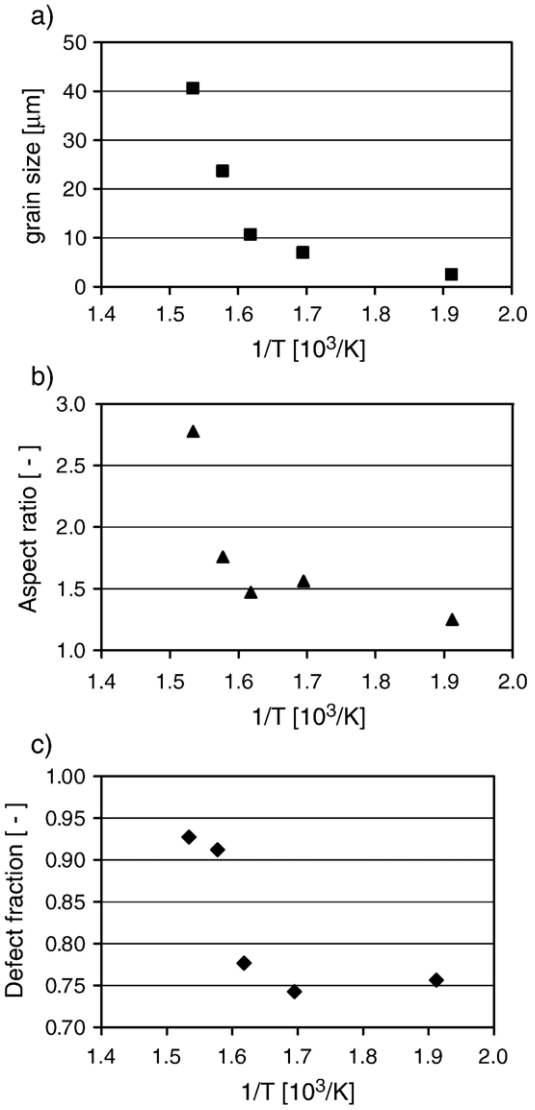

Fig. 18. Plots of microstructural data versus temperature for 5 selected calcite mylonite samples (a) increase of grain size with increasing temperature, (b) increase of aspect ratio with increasing temperature and (c) increase in defect fraction with increasing temperature (see also Table 3).

reflected in an increase in fraction of non-hexagonal grains. An analysis of defect fractions therefore helps in interpreting the development of natural microstructures.

5. Conclusions

We used a 2D microstructural modeling approach to investigate the evolution of defect fraction (i.e. the fraction of non-hexagonal grains) during combined grain boundary migration and deformation to test the hypothesis that strain-induced neighbor switching can result in enhanced grain growth. We conclude the following.

1. Using simple 2D microstructural modeling of grain growth during deformation we were able to produce a component of grain growth not seen under static conditions.
2. This (component of) dynamic grain growth correlates well with a systematic increase in defect fraction, X_d. Starting with a value of 0.71, the defect fraction gradually increases with strain, approaching a constant level around 0.80 at shear strains above ~1.4.
3. Non-linear strain rate sensitivity of dynamic grain growth rate at the lowest and highest strain rates can be linked to microstructural changes in grain topology and geometry, namely varying defect fraction and aspect ratio. This supports the hypothesis that the rate parameter λ in the relation $\dot{d}_{dyn}=\lambda\cdot d\cdot\dot{\varepsilon}$ is strongly related to defect fraction ($\dot{d}_{dyn}$=dynamic grain growth rate, d=grain size and $\dot{\varepsilon}$=strain rate).
4. At relatively low strain rates, dynamic grain growth rate is faster if straining is simulated via inhomogeneous GSS creep rather than by simple homogeneous deformation.
5. At intermediate strain rates, we found a good correlation between our dynamic grain growth rate and strain rate data and already published models and experiments on dynamic grain growth. Both show a constant rate parameter λ. The linear strain rate sensitivity and constant defect fraction (~0.8) observed at intermediate strain rates in this study provides preliminary constraints on the variation of the rate parameter λ.
6. Analysis of defect fraction appears to be a good microstructural tool for establishing whether or not a material has experienced normal static (defect fraction ~0.7) or dynamic (defect fraction ~0.8) grain growth.

Acknowledgements

Mark Jessell is gratefully acknowledged for his help with setting up the ELLE system. Thorough reviews by an anonymous reviewer and especially Marco Herwegh greatly helped to improve the paper. We also thank the editor Neil Mancktelow for his help in preparing the final manuscript.

References

Anderson, M.P., 1988. Simulation of grain growth in two and three dimensions. In: Hansen, N., Jensen, D.J., Leffers, T., Ralph, B. (Eds.), Annealing Processes—Recovery, Recrystallization and Grain GrowthProc. 7th int. Symp. on Metallurgy and Materials Science, pp. 15–34.

Ashby, M.F., Verrall, R.A., 1973. Diffusion-accommodated flow and superplasticity. Acta Metallurgica 21 (2), 149–163.

Atkinson, H.V., 1988. Theories of normal grain growth in pure single phase systems. Acta Metallurgica 36 (3), 469–491.

Barnhoorn, A., Bystricky, M., Burlini, L., Kunze, K., 2004. The role of recrystallisation on the deformation behaviour of calcite rocks: large strain torsion experiments on Carrara marble. Journal of Structural Geology 26 (5), 885–903.

Barr, T.D., Houseman, G.A., 1992. Distribution of deformation around a fault in a non-linear ductile medium. Geophysical Research Letters 19 (11), 1145–1148.

Barr, T.D., Houseman, G.A., 1996. Deformation fields around a fault embedded in a non-linear ductile medium. Geophysical Journal International 125, 473–490.

Bate, P., 2001. The effect of deformation on grain growth in Zener pinned systems. Acta Materialia 49 (8), 1453–1461.

Bergmann, R.B., Shi, F.G., Queisser, H.J., Krinke, J., 1998. Formation of polycrystalline silicon with log-normal grain size distribution. Applied Surface Science 123–124, 376–380.

Bons, P.D., 1993. Experimental deformation of polyphase rock analogues. Geological Ultraiectina 110 (Ph.D. Thesis, Utrecht University), Utrecht, 207 pp.

Bons, P., Urai, J.L., 1992. Syndeformational grain growth: microstructures and kinetics. Journal of Structural Geology 14 (8/9), 1101–1109.

Bons, P.D., Barr, T.D., ten Brink, C.E., 1997. The development of δ-clasts in non-linear viscous materials: numerical approach. Tectonophysics 270, 29–41.

Braun, J., Chéry, J., Poliakov, A., Mainprice, D., Vauchez, A., Tomassi, A., Daignières, M., 1999. A simple parameterization of strain localization in the ductile regime due to grain size reduction: a case study for olivine. Journal of Geophysical Research 104 (B11), 25167–25181.

Burke, J.E., Turnbull, D., 1952. Recrystallization and grain growth in metals. Progress in Metal Physics 3, 220–292.

Bystricky, M., Kunze, K., Burlini, L., Burg, J.-P., 2000. High shear strain of olivine aggregates: rheological and seismic consequences. Science 290, 1564–1567.

Clark, M.A., Alden, T.H., 1973. Deformation enhanced grain growth in a superplastic Sn–1% Bi alloy. Acta Metallurgica 21 (9), 1195–1206.

Dijkstra, A.H., 2001. Deformation and melt in natural mantle rocks: the Hilti Massif (Oman) and the Othris Massif (Greece). Ph.D. Thesis, Utrecht University, Utrecht, 164 pp.

Evans, B., Renner, J., Hirth, G., 2001. A few remarks on the kinetics of static grain growth in rocks. International Journal of Earth Sciences 90, 88–103.

Fayad, W., Thompson, C.V., Frost, H.J., 1999. Steady-state grain-size distributions resulting from grain growth in two dimensions. Scripta Materialia 40 (10), 1199–1204.

Ford, J.M., Wheeler, J., Movchan, A.B., 2002. Computer simulation of grain-boundary diffusion creep. Acta Materialia 50 (15), 3941–3955.

Haslam, A.J., Moldovan, D., Yamakov, V., Wolf, D., Phillpot, S.R., Gleiter, H., 2003. Stress-enhanced grain growth in a nanocrystalline material by molecular-dynamics simulation. Acta Materialia 51 (7), 2097–2112.

Haslam, A.J., Yamakov, V., Moldovan, D., Wolf, D., Phillpot, S.R., Gleiter, H., 2004. Effects of grain growth on grain-boundary diffusion creep by molecular-dynamics simulation. Acta Materialia 52 (7), 1971–1987.

Herwegh, M., Berger, A., 2004. Deformation mechanisms in second-phase affected microstructures and their energy balance. Journal of Structural Geology 26 (8), 1483–1498.

Herwegh, M., De Bresser, J.H.P., Ter Heege, J.H., 2005. Combining natural microstructures with composite flow laws: an improved approach for the extrapolation of lab data to nature. Journal of Structural Geology 27 (3), 503–521.

Hillert, M., 1965. On the theory of normal and abnormal grain growth. Acta Metallurgica 13, 227–238.

Hirth, G., Kohlstedt, D.L., 1995. Experimental constraints on the dynamics of the partially molten upper mantle: deformation in the diffusion creep regime. Journal of Geophysical Research 100 (B2), 1981–2001.

Holm, E.A., Srolovitz, D.J., Cahn, J.W., 1993. Microstructural evolution in two-dimensional two-phase polycrystals. Acta Metallurgica et Materialia 41 (4), 1119–1136.

Holm, K., Embury, J.D., Purdy, G.R., 1977. The structure and properties of microduplex Zr–Nb alloys. Acta Metallurgica 25 (10), 1191–1200.

Jessell, M., Bons, P., Evans, L., Barr, T., Stuwe, K., 2001. Elle: the numerical simulation of metamorphic and deformation microstructures. Computers & Geosciences 27 (1), 17–30.

Jessell, M., Bons, P.D., Evans, B., Piazolo, S., 2004. Numerical experiments into the localization of deformation during recrystallization flow. Material Science Forum 467–470, 647–652.

Jessell, M., Siebert, E., Bons, P.D., Evans, L., 2005. A new type of numerical experiment on the spatial and temporal patterns of localization of deformation in a material with a coupling of grain-size and rheology. Earth and Planetary Science Letters 239 (3–4), 309–326.

Karato, S.I., Paterson, M.S., FitzGerald, J.D., 1986. Rheology of synthetic olivine aggregates: influence of grain size and water. Journal of Geophysical Research 91 (B8), 8151–8176.

Kellermann Slotemaker, A., De Bresser, J.H.P., Spiers, C.J., Drury, M., 2004. Microstructural evolution of synthetic forsterite aggregates deformed to high strain. Material Science Forum 467–470 (Part 1), 579–584.

Kim, B.-N., Hiraga, K., 2000. Simulation of diffusional creep accompanied by grain growth in two-dimensional polycrystalline solids. Acta Materialia 48 (16), 4151–4159.

Kim, B.-N., Hiraga, K., Sakka, Y., Ahn, B.-W., 1999. A grain-boundary diffusion model of dynamic grain growth during superplastic deformation. Acta Materialia 47 (12), 3433–3439.

Krabbendam, M., Urai, J.L., Van Vliet, L.J., 2003. Grain size stabilisation by dispersed graphite in a high-grade quartz mylonite: an example from Naxos (Greece). Journal of Structural Geology 25 (6), 855–866.

Mas, D.L., Crowley, P.D., 1996. The effect of second-phase particles on stable grain size in regionally metamorphosed polyphase calcite marbles. Journal of Metamorphic Geology 14 (2), 155–162.

McDonnell, R.D., Peach, C.J., Spiers, C.J., 1999. Flow behavior of fine-grained synthetic dunite in presence of 0.5 wt% H_2O. Journal of Geophysical Research 104 (B8), 17,823–17,845.

Michibayashi, K., 1993. Syntectonic development of a strain-independent steady-state grain size during mylonitization. Tectonophysics 222, 151–164.

Montesi, L.G.J., Hirth, G., 2003. Grain size evolution and the rheology of ductile shear zones: from laboratory experiments to postseismic creep. Earth and Planetary Science Letters 211 (1–2), 97–110.

Olgaard, D.L., 1990. The role of second phase in localizing deformation. In: Knipe, R.J., Rutter, E.H. (Eds.), Deformation Mechanisms, Rheology and Tectonics. Geological Society Special Pubications. Geological Society of London, London, United Kingdom, pp. 175–181.

Piazolo, S., 2001. Shape fabric development during progressive deformation. Ph.D. Thesis, Johannes Gutenberg-Universität, Mainz, 251 pp.

Piazolo, S., Bons, P.D., Jessell, M.W., Evans, L., Passchier, C.W., 2002. Dominance of microstructural processes and their effect on microstructural development: insights from numerical modeling of dynamic recrystallization. In: De Meer, S., Drury, M.R., De Bresser, J.H.P., Pennock, G.M. (Eds.), Deformation Mechanisms, Rheology and Tectonics: Current Status and Future Perspectives. Special Publications, vol. 200. Geological Society, London, pp. 149–170.

Pieri, M., Burlini, L., Kunze, K., Stretton, I., Olgaard, D.L., 2001. Rheological and microstructural evolution of Carrara marble with high shear strain: results from high temperature torsion experiments. Journal of Structural Geology 23, 1393–1413.

Rabinovich, M.K., Trifonov, V.G., 1996. Dynamic grain growth during superplastic deformation. Acta Materialia 44 (5), 2073–2078.

Ranalli, G., 1984. Grain size distribution and flow stress in tectonites. Journal of Structural Geology 6 (4), 443–447.

Rutter, E.H., 1995. Experimental study of the influence of stress, temperature, and strain on the dynamic recrystallization of Carrara marble. Journal of Geophysical Research 100 (B12), 24,651–24,664.

Rutter, E.H., 1998. Use of extension testing to investigate the influence of finite strain on the Theological behaviour of marble. Journal of Structural Geology 20 (2–3), 243–254.

Sato, E., Kuribayashi, K., Horiuchi, R., 1990. A mechanism of superplastic deformation and deformation induced grain growth based on grain switching. Materials Research Society Symposium Proceedings 196, 27–32.

Seidensticker, J.R., Mayo, M.J., 1998a. Dynamic and static grain growth during the superplastic deformation of 3Y-TZP. Scripta Materialia 38 (7), 1091–1100.

Seidensticker, J.R., Mayo, M.J., 1998b. A topological rationale for the dependence of grain growth on strain during superplastic deformation. Acta Materialia 46 (14), 4883–4893.

Schmid, S.M., Boland, J.N., Paterson, M.S., 1977. Superplastic flow in fine grained limestone. Tectonophysics 43 (3–4), 257–291.

Schmid, S.M., Panozzo, R., Bauer, S., 1987. Simple shear experiments on calcite rocks: rheology and microfabric. Journal of Structural Geology 9, 747–778.

Sherwood, D.J., Hamilton, C.H., 1992. Production of cellular defects contributing to deformation-enhanced grain growth. Scripta Metallurgica et Materialia 27 (12), 1771–1776.

Sherwood, D.J., Hamilton, C.H., 1994. The neighbourswitching mechanism of superplastic deformation: the constitutive relationship and deformation-enhanced grain growth. Philosophical Magazine 70, 109–143.

Ter Heege, J.H., De Bresser, J.H.P., Spiers, C.J., 2004. Composite flow laws for crystalline materials with log-normally distributed grain size: theory and application to olivine. Journal of Structural Geology 26 (9), 1693–1705.

Ter Heege, J.H., De Bresser, J.H.P., Spiers, C.J., 2005. Dynamic recrystallization of wet synthetic polycrystalline halite: dependence of grain size distribution on flow stress, temperature and strain. Tectonophysics 396 (1–2), 35–57.

Urai, J.L., Jessell, M., 2001. Recrystallization and grain growth in minerals: recent developments. In: Gottstein, G., Molodov, D. (Eds.), Recrystallization and Grain Growth. Proceedings of the First Joint International Conference. Springer Verlag, RWTH Aachen, Germany, pp. 87–96.

Von Neumann, J., 1952. Discussion to 'Grain shapes and other metallurgical applications of topology' by C.S. Smith. In: Brick, R.M. (Ed.), Metal Interfaces. ASM, Cleveland, Ohio, pp. 108–110.

Walker, A.N., Rutter, E.H., Brodie, K.H., 1990. Experimental study of grain-size sensitive flow of synthetic, hot-pressed calcite rocks. In: Knipe, R.J., Rutter, E.H. (Eds.), Deformation mechanisms, rheology and tectonics. Geological Society Special Publications. Geological Society of London, London, United Kingdom, pp. 259–284.

Weaire, D., Kermode, J.P., 1983. Computer simulation of a two-dimensional froth: I. Method and motivation. Philosophical Magazine. B 48 (No.3), 245–259.

Wilkinson, D.S., Caceres, C.H., 1984. On the mechanism of strain-enhanced grain growth during superplastic deformation. Acta Metallurgica 32 (9), 1335–1345.

Yamasaki, T., 2004. Localized rheological weakening by grain-size reduction during lithospheric extension. Tectonophysics 386 (3–4), 117–145.

Zhilyaev, A.P., Kim, B.-K., Szpunar, J.A., Baro, M.D., Langdon, T.G., 2005. The microstructural characteristics of ultrafine-grained nickel. Materials Science & Engineering. A, Structural Materials: Properties, Microstructure and Processing 391 (1–2), 377–389.